Journal of Biomedical Optics

BiomedicalOptics.SPIEDigitalLibrary.org

Probe for evaluating the absorbing and transport scattering properties of turbid fluids using low-cost time-of-flight technology

Jeremy C. Hebden
Ruchir Shah
Danial Chitnis

SPIE.

Jeremy C. Hebden, Ruchir Shah, Danial Chitnis, "Probe for evaluating the absorbing and transport scattering properties of turbid fluids using low-cost time-of-flight technology," *J. Biomed. Opt.* **22**(5), 055009 (2017), doi: 10.1117/1.JBO.22.5.055009.

Probe for evaluating the absorbing and transport scattering properties of turbid fluids using low-cost time-of-flight technology

Jeremy C. Hebden,* Ruchir Shah, and Danial Chitnis
University College London, Department of Medical Physics and Biomedical Engineering, London, United Kingdom

Abstract. A probe is described that when immersed into a highly scattering fluid provides a measurement of its scattering and absorbing properties at a single optical wavelength. It uses recently available low-cost proximity sensor modules to estimate the mean flight times of photons diffusely transmitted between near-infrared sources and detectors at two different separations. The probe has been designed with a specific application for enabling the rapid and efficient production of fluids, which mimic the optical properties of biological tissues. The potential of the device is demonstrated using precalibrated solutions of intralipid, an intravenous nutrient, and absorbing dye. It is shown that a combination of time-of-flight measurements at two source–detector separations can uniquely specify the absorption coefficient and the transport scattering coefficient. [DOI: 10.1117/1.JBO.22.5.055009]

Keywords: biomedical optics; diffusion; tissues; optical properties.

Paper 170075R received Jan. 31, 2017; accepted for publication May 9, 2017; published online May 25, 2017.

1 Introduction

The development and evaluation of instruments for biomedical optics applications frequently require the use of objects that mimic the optical properties of biological tissues, known as phantoms.[1] The primary interactions between light and tissue at optical wavelengths are absorption and scatter, and the degree to which each occurs in a synthetic medium can be easily manipulated by an appropriate combination of scattering and absorbing agents within a solid or liquid matrix. Phantoms are most often used for applications in optical spectroscopy, imaging, and dosimetry where sources and detectors are placed on the surface of tissue with separations between a few millimeters and several centimeters. At commonly used near-infrared (NIR) wavelengths, scatter dominates over absorption and light propagating more than a millimeter or so in tissue is rendered diffuse, i.e., all initial source beam directionality information is lost. Under these conditions, it is sufficient for phantoms to mimic the so-called transport scattering properties of tissue, characterized by the transport (or "reduced") scattering coefficient denoted by μ_s', with units of mm^{-1}.[1] Meanwhile, absorption, which has much stronger wavelength dependence in tissue than scatter, is characterized by the absorption coefficient μ_a, also with units of mm^{-1}.

Many of the phantoms employed to date have consisted of liquids (usually water based), in which suitable absorbing (e.g., inks, molecular dyes, and hemoglobin) and scattering (e.g., lipids, powdered solids, and microspheres) agents are added.[2–4] The construction of solid phantoms also often involves adding agents to a liquid matrix (e.g., resins, rubbers, gels, etc.) before solidifying (e.g., by the addition of a catalyst).[5–8] A broad variety of phantom recipes have been devised, and each usually relies on producing precise concentrations of absorbing and scattering substances, which have had their optical properties accurately characterized in advance.

In this paper, we describe a low-cost tool for producing fluids with tissue-like optical properties without the need for prior characterization of the scattering and absorbing agents. In principle, the tool can be produced in the form of a "dipstick" that provides an instantaneous measure of μ_a and μ_s' during the mixing of the components. Although such a concept has been proposed and explored before, most recently by Zhou et al.,[9] previous investigations have focused either on measurements of intensity (i.e., diffuse reflectance or transmittance) or have required complex and expensive bench-top systems based on time-domain[10] or frequency-domain measurements.[11] Measurements of intensity are notoriously influenced by the coupling between the optical sources/detectors and the medium; for example, a small stain, scratch, or air bubble on the surface of the probe would be likely to corrupt the measurement. However, time-domain measurements (of times-of-flight of photons emitted by a pulsed source) and frequency-domain measurements (of phase delay from an intensity-modulated source) are largely immune from variation in coupling. The device described here is based on a very low-cost commercial time-of-flight proximity sensor developed for the mobile phone market.

2 Theory

Light propagation through media in which scattering dominates over absorption can be modeled using the time-dependent diffusion equation. Arridge et al.[12] show that for a point source and point detector separated by a distance d in an infinite homogeneous diffusing medium (where $d \gg 1/\mu_s'$), the mean time-of-flight of photons $\langle t \rangle$ is given as

*Address all correspondence to: Jeremy C. Hebden, E-mail: j.hebden@ucl.ac.uk

$$\langle t\rangle = \frac{d^2}{2\left(\gamma^2 + d\gamma\sqrt{\mu_a c}\right)}, \tag{1}$$

where c is the velocity of light in the medium and γ is given as

$$\gamma^2 = \frac{c}{3(\mu_a + \mu_s')}. \tag{2}$$

A measurement of flight times of photons traveling through a highly scattering medium yields a broad distribution sometimes known as a temporal point spread function,[12] of which $\langle t\rangle$ is the weighted average flight time. Combining these equations, it can be shown that

$$\mu_s' = \frac{4c}{3d^2} \Big/ \left(\sqrt{\mu_a c + \frac{2}{\langle t\rangle}} - \sqrt{\mu_a c}\right) - \mu_a. \tag{3}$$

Thus, μ_s' can be calculated from a single measurement of $\langle t\rangle$ at separation d if both μ_a and c are known. For most phantom measurements, it is likely that c is known, or if not it can be measured separately or estimated with reasonable precision. However, if μ_a is not known, it can be evaluated using measurements of $\langle t\rangle$ at two or more values of distance d. For example, for two measurements of mean time $\langle t\rangle_1$ and $\langle t\rangle_2$ obtained using two different separations d_1 and d_2, respectively, μ_s' can be eliminated from Eq. (3) to obtain

$$\mu_a = \left[\left(\frac{d_2}{d_1}\right)^2 \frac{\langle t\rangle_1}{\langle t\rangle_2} + \left(\frac{d_1}{d_2}\right)^2 \frac{\langle t\rangle_2}{\langle t\rangle_1} - 2\right] \Big/ 2c\left[\langle t\rangle_1\left(1 - \frac{d_2}{d_1}\right) + \langle t\rangle_2\left(1 - \frac{d_1}{d_2}\right)\right]. \tag{4}$$

The corresponding value of μ_s' can then be derived by inserting the calculated value of μ_a into Eq. (3).

The above analysis assumes ideal point sources and detectors in an infinite homogenous medium. The assumption of infinite extent to a fluid medium is likely to be approximated in practice providing the distances between the nearest boundary of the container and the source and the detector are at least a few times larger than the separation d. However, for any practical measuring device, the presence of optical components within the fluid will violate the condition of homogeneity. Consequently, a direct application of the above formulas is unlikely to be successful, although it may be sufficient to utilize a precalibrated lookup table to convert time-of-flight measurements to values of μ_s' and μ_a. While statistical uncertainties in measurements of $\langle t\rangle$ will inevitably compromise the accuracy and uniqueness of the solutions, both may be improved by combining data acquired at additional separations.

3 Experimental Measurements

3.1 *Proximity Sensor*

While time-of-flight measurements of light transmitted across biological tissues and other highly scattering media have been performed for several decades,[13] only recently has technology become available that can do this at negligible cost. The ST Microelectronics VL6180X proximity sensor uses photon flight time information to measure the distance between the sensor and a reflecting surface.[14] The sensor incorporates a vertical cavity surface-emitting laser source with an emission wavelength of 850 nm, and a single-photon avalanche diode detector on a single chip, 3.3-mm apart. The specified distance range is 0 to 100 mm with a resolution of 1 mm, although ranging beyond 100 mm is quoted as possible with less reliability. The $2 sensor is available with an evaluation kit enabling USB connection to a PC, and the software provided enables distance measurements (mm) and detected photon count rates (Mcps) to be acquired at a rate of 10 Hz.

3.2 *Sensor Characterization*

To verify the measurement accuracy of the proximity sensor in air, the sensor was supported vertically while a parallel sheet of white board, serving as a diffusely reflecting target, was held at a known distance from the sensor, as shown in Fig. 1. Data from the sensor were recorded for 100 s at each distance as the board was translated in 5-mm steps away from the sensor. An average distance measurement was calculated and then the data were divided into 10 segments of 10 s each to calculate a standard deviation. The recorded values of distance and photon count rate are plotted against the true sensor-board distance from the target in Fig. 2. Error bars represent the standard deviation for a 10-s (100 samples) measurement at each position.

The plot of true versus measured distance exhibits a strong linearity with a slope of 0.999 ± 0.011 and an intercept of zero [linear fit shown in Fig. 2(a)]. The intensity data exhibit a rapid decrease in the detected signal due to the divergence of the emitted light and nonspecular reflectance of the white board.

3.3 *Single Sensor Measurement in a Turbid Fluid*

To assess the ability of the sensor to measure photon flight time across a region of highly scattering fluid, a tank of intralipid was prepared. Intralipid is a milk-like commercially available lipid emulsion produced as an intravenous nutrient and is commonly used as a phantom material.[2] The rectangular tank had a surface area of 200×130 mm^2 and was filled to a depth of 50 mm with a precalibrated solution of intralipid to produce a fluid with a transport scatter coefficient of 1.0 mm^{-1} and absorption of 0.0043 mm^{-1} at the sensor wavelength of 850 nm.

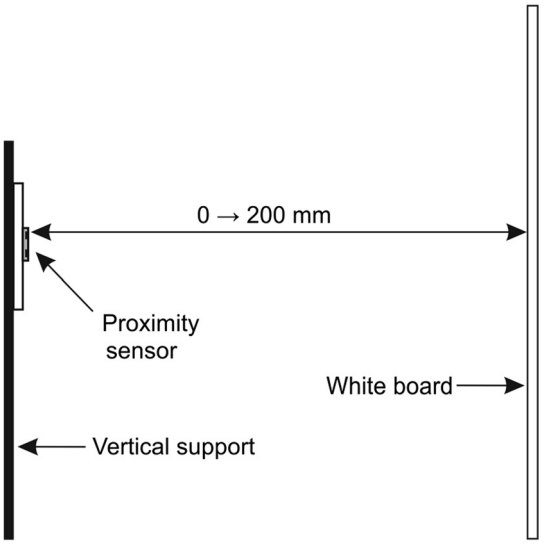

Fig. 1 Measurement of the distance between the VL6180X sensor and a reflecting white board.

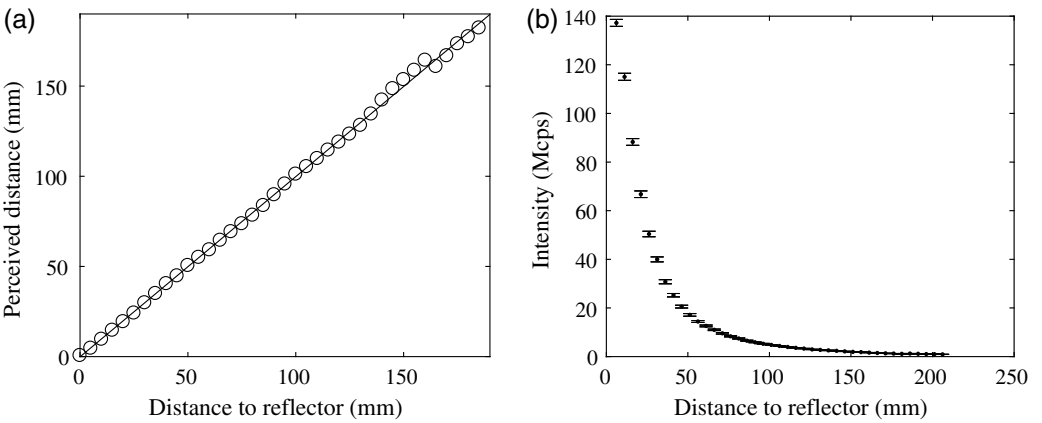

Fig. 2 (a) Distance and (b) intensity values obtained using the VL6180X sensor.

To facilitate measurements in the fluid for different source–detector separations, a small customized connector was developed (3-D printed in black plastic) to secure the ends of two short (37 mm) lengths of unterminated polymer optical fiber (diameter 1 mm) in contact with the source and detector. The other ends of the fibers were held apart using a spacer, consisting of a thin plastic rod with two holes separated by a fixed distance d. This is shown in Fig. 3. The ends of the fibers were immersed to a depth approximately halfway between the top and bottom surfaces of the fluid, and data were recorded for 10 s for spacers with separations of 4, 6, 10, 14, and 18 mm. The resulting data are shown in Fig. 4.

The distance m measured by the sensor exhibits a smooth, near-linear increase with fiber separation, while the intensity shows a corresponding exponential-like decrease. However, it was noted that when the intensity falls below 1 Mcps, the distance measurements become erratic and exhibit some correlation with the intensity. Consequently, it was ensured that the measured intensity remained above 1 Mcps for all subsequent experiments.

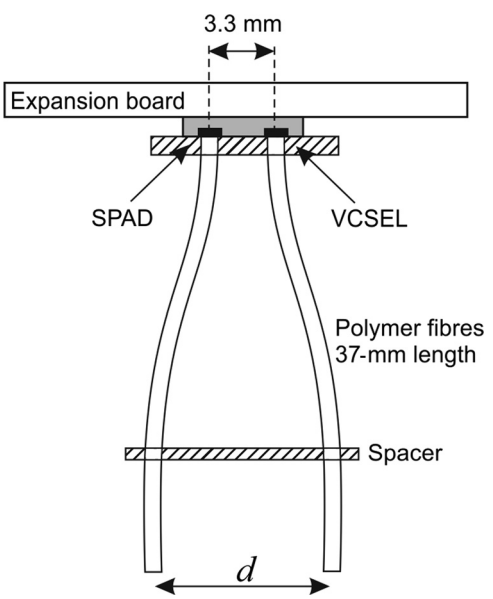

Fig. 3 A customized connector securing two short lengths of polymer fiber in contact with the VL6180X sensor source and detector.

The continuous line in Fig. 4(a) represents the theoretical mean photon pathlength ($c\langle t\rangle$) calculated using Eq. (1). There are two reasons why a close match between the measured and modeled distances is not expected. First, and most importantly, the sensor was designed to measure distances in air and not to provide a distance value from a (deliberately) temporally broadened signal from highly scattered light. Information on the measurement technique and signal processing scheme employed by the sensor is not in the public domain, and there is no reason to expect the sensor to yield the mean photon pathlength. Second, the measurement geometry does not closely approximate a point source and point detector in an infinite medium. In principle, this could be improved using longer and thinner fibers embedded in a larger tank, although the finite depth range of the sensor restricts the maximum length of the fibers that can be employed.

3.4 *Dual Sensor Measurement in a Turbid Fluid*

Pairs of fibers were attached to two independent sensors mounted on different expansion boards. Spacers of 3 and 6 mm were attached to the ends of the two pairs, which were then immersed into the same tank ~90 mm apart (sufficient to enable the sensors to be operated simultaneously). Measurements were acquired for solutions with nine different intralipid concentrations, corresponding to transport scattering coefficients (at 850 nm) between 0.4 and 2.0 mm^{-1}, increasing in steps of 0.2 mm^{-1}. For each intralipid concentration, an aqueous solution of NIR-absorbing dye (ICI S109564) was manually injected and stirred into the fluid to increase its absorption coefficient (at 850 nm) in steps of 0.001 to 0.04 mm^{-1}. Measurements were acquired from both sensors, averaging over 100 samples. The result was pairs of distance measurements m_1 and m_2 for $9 \times 41 = 369$ fluids with distinct optical properties.

Figure 5 shows the distance values obtained using one sensor (m_1 with fiber separation $d_1 = 6$ mm) plotted against the distance values obtained using the other sensor (m_2 with $d_2 = 3$ mm). A constant offset is subtracted from both sets of measurements, equal to the distance recorded when the two ends of the fibers are coupled together (i.e., representing zero flight time). As expected, Fig. 5 shows nine lines of 41 points each corresponding to the different values of μ_s' and μ_a. The spacing between points within a given line decreases significantly as μ_a increases, and to a lesser extent the spacing among lines tends to decrease as μ_s' increases.

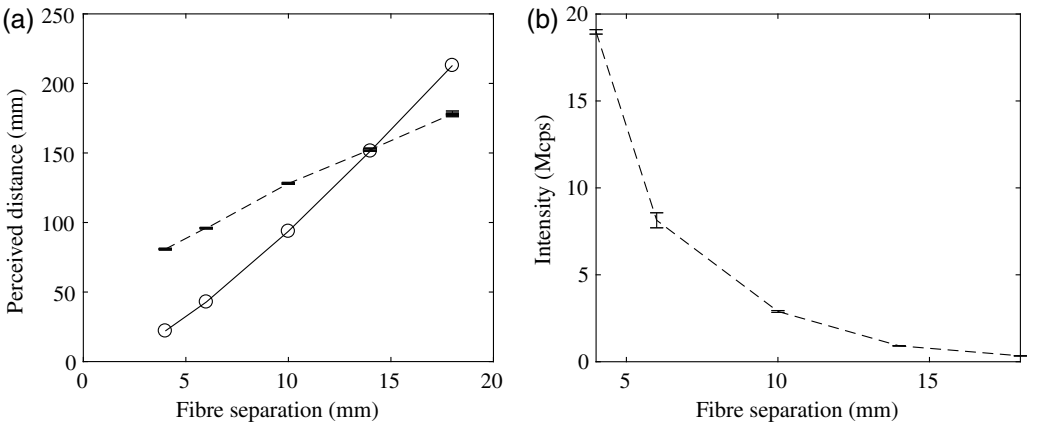

Fig. 4 (a) Distance and (b) intensity values recorded in intralipid for five different fiber separations. The continuous line represents in (a) is the mean photon pathlength estimated using Eq. (1).

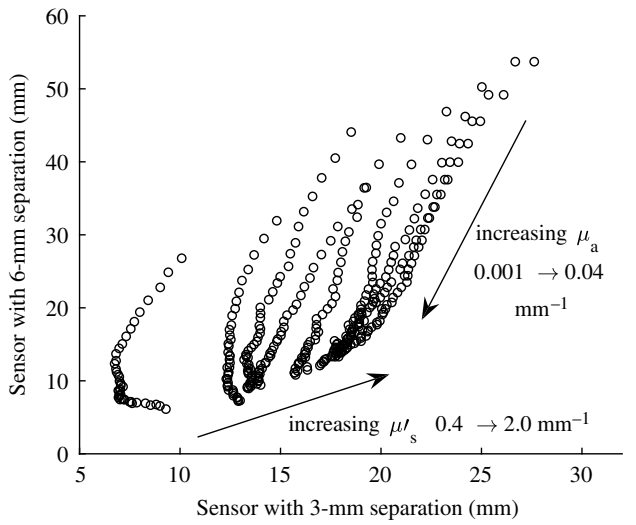

Fig. 5 A scatter plot of the distance measurements acquired using the two fiber separations for the 369 different fluids.

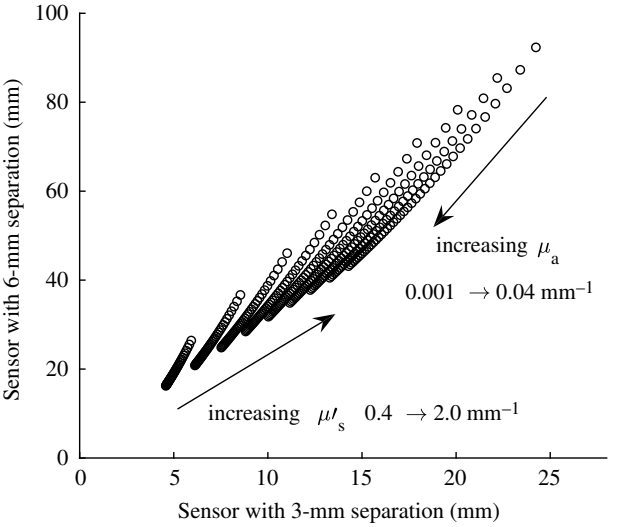

Fig. 6 A scatter plot of the mean pathlengths estimated using Eq. (1) for the two fiber separations and the 369 different fluids.

For comparison, Fig. 6 shows the corresponding theoretical values of mean pathlength ($c\langle t\rangle$) calculated using Eq. (1) for the same two source–detector separations and the 369 pairs of optical properties used experimentally. The ranges of distances for the two sensors are similar to those exhibited experimentally. Again, differences between the theory and experimental data are inevitable for the reasons stated above; although it is actually encouraging that the points show less overlap in the experimental data than predicted by the diffusion model.

Despite some similarities between Figs. 5 and 6, the comparison confirms that the theoretical model is not sufficient to enable the optical properties μ_s' and μ_a to be extracted from the distance measurements directly by applying Eqs. (3) and (4). Nevertheless, the relatively little overlap of data (except at very high μ_a) in Fig. 5 suggests that empirical models can be applied to enable reasonably accurate predictions of both properties to be extracted for an arbitrary pair of distance values. For example, a lookup table can be generated by extrapolating between points on the surfaces of plots of $\mu_s'(m_1, m_2)$ and $\mu_a(m_1, m_2)$. To compensate for noise in the data, a polynomial or spline function can be fitted in two dimensions to provide a smoother interpolation. This idea was briefly explored by obtaining a simple two-dimensional third-order polynomial (i.e., 10 parameters) fit to our data. The average differences between the measured values of μ_s' and μ_a and the values predicted by the polynomial fit were 9% and 18%, respectively, with the largest errors occurring at the highest values of both coefficients (i.e., where most overlap of points occurs in Fig. 5).

4 Discussion

The recent advent of low-cost solid-state time-of-flight technology has the potential to find a vast new breadth of uses. Applications identified for the mobile phone market have enabled mass production of the proximity sensor evaluated here to be sold at nominal cost. This sensor has evident limitations for characterizing the optical properties of turbid fluids. It is not designed to measure the temporal broadening produced by scatter; almost certainly it does not compute a true measurement of mean photon pathlength, although the measured distance appears to correlate quite well. The emitted power is low and the detection area is small, which limits the distance measurement range, and the wavelength is fixed at 850 nm. Despite these

limitations, the combination of two sensors enables a pair of measures to be acquired, which appear to uniquely characterize absorption and transport scattering properties of turbid intralipid-based solutions, at least when the absorption is comparatively low.

Because of the limited sensitivity of the sensor, it was necessary to use small source–detector separations of $d_1 = 3$ mm and $d_2 = 6$ mm. Consequently, measurements at the lowest values of μ_s' will not have met the diffusion equation condition that $d \gg 1/\mu_s'$, which explains the observed departure between the experimental results and the theoretical model as μ_s' decreases. However, we note that since this work was completed, ST Microelectronics have released their VL53L0X proximity sensor[15] that has a larger specified range of 2 m but emits at 940 nm, which is less suitable for NIR spectroscopy and imaging.

The sensors can easily be integrated into a "dipstick" with a geometry more suitable for quickly characterizing phantom fluids. Ideally, larger source–detector separations would be employed and the combination of three or more measurements is likely to yield superior accuracy in the measurement of both coefficients. Such a device might also find other applications for characterizing scattering fluids, such as paint, milk and other liquid foods, industrial solvents, and liquid pharmaceuticals.

Recent advances in the field of miniaturized time-correlated single-photon counting devices[16] and solid-state sources of very short pulses of light have already begun to be explored in applications in NIR spectroscopy and imaging, particularly by research groups in Milan[17] and Lausanne/Zurich.[18]

Disclosures

The authors have no relevant financial interests in the paper and no other potential conflicts of interest.

Acknowledgments

This work was funded in part by EPSRC Grants Nos. EP/K020315/1 and EP/J0201318/1. The authors would like to thank Samuel Searles-Bryant for performing some of the initial measurements and Laura Dempsey for assistance with the preparation of fluids.

References

1. B. W. Pogue and M. S. Patterson, "Review of tissue simulating phantoms for optical spectroscopy, imaging and dosimetry," *J. Biomed. Opt.* **11**, 041101 (2006).
2. S. T. Flock et al., "Optical properties of intralipid: a phantom medium for light propagation studies," *Lasers Surg. Med.* **12**, 510–519 (1992).
3. S. J. Madsen, M. S. Patterson, and B. C. Wilson, "The use of India ink as an optical absorber in tissue-simulating phantoms," *Phys. Med. Biol.* **40**, 955–961 (1995).
4. E. L. Hull, M. G. Nichols, and T. H. Foster, "Quantitative broadband near-infrared spectroscopy of tissue-simulating phantoms containing erythrocytes," *Phys. Med. Biol.* **43**, 3381–3404 (1998).
5. M. Firbank, M. Oda, and D. T. Delpy, "An improved design for a stable and reproducible phantom material for use in near-infrared spectroscopy and imaging," *Phys. Med. Biol.* **40**, 955–961 (1995).
6. U. Sukowski et al., "Preparation of solid phantoms with defined scattering and absorption properties for optical tomography," *Phys. Med. Biol.* **41**, 1823–1844 (1996).
7. M. L. Vernon et al., "Fabrication and characterisation of a solid polyurethane phantom for optical imaging through scattering media," *Appl. Opt.* **38**, 4247–4251 (1999).
8. M. Lualdi et al., "A phantom with tissue-like optical properties in the visible and near-infrared for use in photomedicine," *Lasers Surg. Med.* **28**, 237–243 (2001).
9. Y. Zhou et al., "An integrated fiber-optic probe combined with support vector regression for fast estimation of optical properties of turbid media," *Anal. Chim. Acta* **880**, 122–129 (2015).
10. M. S. Patterson, B. Chance, and B. C. Wilson, "Time resolved reflectance and transmittance for the non-invasive measurement of tissue optical properties," *Appl. Opt.* **28**, 2331–2336 (1989).
11. J. B. Fishkin et al., "Frequency-domain method for measuring spectral properties in multiple-scattering media: methemoglobin absorption spectrum in a tissuelike phantom," *Appl. Opt.* **34**, 1143–1155 (1995).
12. S. R. Arridge, M. Cope, and D. T. Delpy, "The theoretical basis for the determination of optical pathlengths in tissue: temporal and frequency analysis," *Phys. Med. Biol.* **37**, 1531–1560 (1992).
13. J. C. Hebden, S. R. Arridge, and D. T. Delpy, "Optical imaging in medicine: I. Experimental techniques," *Phys. Med. Biol.* **42**, 825–840 (1997).
14. "VL6180X Data sheet," ST Microelectronics, http://www.st.com/resource/en/datasheet/vl6180x.pdf (16 March 2016).
15. "VL53L0X Data sheet," ST Microelectronics, http://www.st.com/resource/en/datasheet/vl53l0x.pdf (30 May 2016).
16. N. A. W. Dutton et al., "A time-correlated single-photon-counting sensor with 14GS/S histogramming time-to-digital converter," in *IEEE Int. Solid-State Circuits Conf.* (2015).
17. A. Tosi et al., "Fast-gated single-photon counting technique widens dynamic range and speeds up acquisition time in time-resolved measurements," *Opt. Express* **19**, 10735 (2011).
18. J. M. Pavia et al., "A 1×400 backside-illuminated SPAD sensor with 49.7 ps resolution, 30 pJ/sample TDCs fabricated in 3D CMOS technology for near-infrared optical tomography," *IEEE J. Solid-State Circuits* **50**, 2406–2418 (2015).

Jeremy C. Hebden is a professor of biomedical optics at the University College London, where he is currently the head of the Department of Medical Physics and Biomedical Engineering and director of the Biomedical Optics Research Laboratory. He received his BSc and PhD degrees from Imperial College London in 1981 and 1984, respectively. His research interests include the development of optical systems for imaging the brains of newborn infants.

Ruchir Shah performed this work while taking an intercalated BSc in medical sciences with medical physics and bioengineering at University College London, from which he graduated in 2016. He is currently engaged in clinical training as a medical student, also at University College London.

Danial Chitnis received his BSc in electronics engineering from Chamran University of Ahvaz, Iran, in 2007, an MSc in microelectronics and system engineering from the University of Bristol in 2009, and a DPhil in engineering science from the University of Oxford in 2013. He then joined the UCL Department of Medical Physics and Biomedical Engineering to develop optical brain imaging systems. His research interests include CMOS circuits and optical detectors, especially single photon avalanche diodes.